Performance of the Prototype of the Charged-Particle Veto System of the PADME Experiment

F. Ferrarotto, L. Foggetta, G. Georgiev, P. Gianotti, V. Kozhuharov, E. Leonardi, G. Piperno, M. Raggi, C. Taruggi, L. Tsankov, and P. Valente

***Abstract*— The PADME experiment will search for the $e^+e^- \to \gamma A'$ process in a positron-on-target experiment, assuming a decay of the A' into invisible particles of the hidden sector. The 550-MeV positron beam of the DAΦNE beam-test facility (BTF), at Laboratori Nazionali di Frascati, Istituto Nazionale di Fisica Nucleare, will be used. The suppression of the background, due to bremsstrahlung emission from the beam positrons, requires highly efficient charged-particle detectors with optimized geometry. A fine-grained plastic scintillator veto composed of three stations operating in vacuum is proposed. Two stations, placed inside a dipole magnet with 0.6-T magnetic field, will also provide momentum measurement at the percent level. Different prototypes for the design of the detector elements, the photosensor, and the front-end electronics were studied with single electron beam at the DAΦNE BTF to choose the optimal technologies and construction solutions. PADME is currently under construction, and it is planned to begin data collection in 2018. The design of the charged-particle vetoes and the test beam performance of the prototypes are reviewed.**

***Index Terms*— Position sensitive particle detectors, Scintillation counters, Time measurement.**

I. Introduction

THE existence of new light and neutral degrees of freedom is predicted in many extensions of the standard model (SM) of particle physics [1]. Recently, the interest to probe them experimentally has increased since they may shed light on the nature of dark matter and its interaction with the SM particles. One of the simplest possible scenarios is to consider a completely new sector of particles, which are neutral with respect to the SM gauge groups. Any interaction between this hidden sector and the visible sector is mediated by a new interaction, $U'(1)$ in the simplest case, and the corresponding gauge boson A' is called the dark photon. The strength of the interaction between A' and the visible sector is suppressed by a large factor, which may also be generated through kinetic mixing between A' and the ordinary photon. The expected A' phenomenology depends on the masses of the particles and the coupling constants in the hidden sector and varies from A' decaying with almost 100% probability to e^+e^- pairs to A' being almost completely invisible with a dominant $\chi\bar{\chi}$ final state, where χ is a hidden-sector particle. This rich phenomenology, and the possible explanation of various discrepancies between theory and experiment, motivates the proposal of new experiments devoted to the search of A'.

The PADME experiment is planned to be operational in April 2018 at the DAΦNE Linac [2], [3] and aims to search for the new neutral particles produced in the electron–positron annihilation process. The primary process of interest is

$$e^+ + e^- \to \gamma + A'. \tag{1}$$

Assuming A' decays into invisible final states, the only kinematic property that can be reconstructed is the so-called missing mass squared

$$M^2_{\text{miss}} = (P_{e^+} + P_{e^-} - P_\gamma)^2 \tag{2}$$

where P_i is the four-momentum of the particle i. In presence of A', the missing mass distribution will peak at a value equal to $M^2_{A'}$, while the expected background will be a continuous distribution over the studied mass range.

The PADME approach employs a positron beam, from the DAΦNE linear accelerator, which will impinge on a thin target. Thus, the electrons are assumed to be at rest, $P_{e^-} = (m_e, 0, 0, 0)$, while the positron momentum is determined from the beam parameters. The DAΦNE Linac will provide positrons with intensities of about 5000 e^+ per bunch and energies up to 550 MeV with repetition rate of 49 Hz [7].

The major components of the PADME experiment, shown in Fig. 1, are listed as follows.

Manuscript received February 15, 2018; revised March 28, 2018; accepted March 28, 2018. Date of publication April 3, 2018; date of current version August 15, 2018. This work was supported in part by BG-NSF under Grant DN-08/14 from 12.2016 and and in part by MoU 70-06-497/07-10-2014 between Sofia University and LNF-INFN. *(Corresponding authors: G. Georgiev; V. Kozhuharov.)*

F. Ferrarotto, E. Leonardi, and P. Valente are with the Istituto Nazionale di Fisica Nucleare Sezione di Roma, 00185 Rome, Italy.

L. Foggetta, P. Gianotti, and G. Piperno are with the Laboratori Nazionali di Frascati, 00044 Frascati, Italy.

G. Georgiev and V. Kozhuharov are with the Faculty of Physics, University of Sofia "St. Kliment Ohridski," 1164 Sofia, Bulgaria, and also with the Laboratori Nazionali di Frascati, 00044 Frascati, Italy (e-mail: georgi.stefanov.georgiev@cern.ch).

M. Raggi is with the Sapienza Università di Rome, 00185 Rome, Italy, and also with the Istituto Nazionale di Fisica Nucleare Sezione di Roma, 00185 Rome, Italy.

C. Taruggi is with the Università di Roma "Tor Vergata," I-00133 Rome, Italy, and also with the Laboratori Nazionali di Frascati, 00044 Frascati, Italy.

L. Tsankov is with the Faculty of Physics, University of Sofia "St. Kliment Ohridski," 1164 Sofia, Bulgaria.

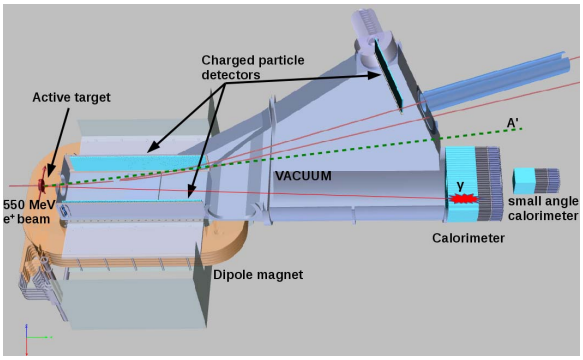

Fig. 1. Cross section of the PADME experiment.

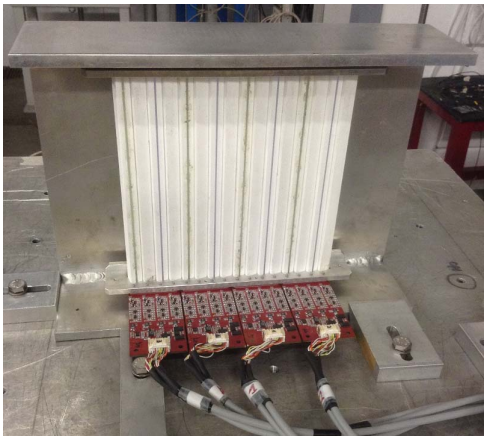

Fig. 2. PADME veto prototype placed on the BTF remotely movable table.

- *Active Target:* Incident positrons interact in a 100-μm-thick active target made of polycrystalline diamond. The target is also used to measure the average beam position, time and intensity.
- *Calorimeters:* Two electromagnetic calorimeters measure the energy of the photons and are also used to veto the standard annihilation events [5].
- *Charged-Particle Detectors:* A set of segmented charged-particle detectors, placed inside of a dipole magnet, are used to detect positrons, which undergo significant energy loss in the target. In addition, these detectors allow to search for dark-photon decays into visible pairs [4].

The experiment is enclosed in a large vacuum chamber to prevent the unwanted particle interactions with ambient air.

A prototype study of the charged-particle veto is discussed further in this paper.

II. PADME Charged-Particle Veto

The cross section for process (1) is suppressed with a large factor with respect to the ordinary two-photon annihilation. In addition, the only detectable particle in the final state is the recoil photon. The cross section for two-photon annihilation of a positron on a carbon target is $\sigma_{\text{annih}} = 1.55$ mb while the cross section for radiative photon emission is $\sigma_{\text{brems}} = 4000$ mb in the field of a nucleus and 188 mb in the field of atomic electrons, for $E_\gamma > 1$ MeV. Since also the bremsstrahlung is characterized by a single photon in the final state, the only possibility to suppress this type of background in the search for A' is to detect the final state positron.

For this purpose, a set of three segmented detectors, placed inside the vacuum vessel, will be used in PADME. Two of them will be placed inside the dipole magnet of the experiment and will serve to detect positrons (PVeto) and electrons (EVeto) with the momentum in the range 50–450 MeV. Another detector will be placed further downstream and will serve to cover the range 450–550 MeV for positrons. The time resolution for these detectors is required to be less than 1 ns. Time measurement with such precision, according to Monte Carlo (MC) simulation, serves to match clusters in the calorimeters with hits in the positron veto, thus allowing to suppress the background from hard bremsstrahlung of the beam particles. Vetoes are expected to detect charged particles with efficiency higher than 99% [2]. The necessary segmentation of the charged-particle vetoes was determined from the requirement that they have to provide the momentum resolution matching the energy resolution of the calorimeter 6.5% for photons with the energy of 100 MeV, according to MC simulation [2], [5]. The detectors will be made of plastic scintillator bars with 10×10 mm^2 cross section and 200 mm length, placed vertically with respect to the beam line. The emitted light will be detected by the silicon photomultipliers (SiPM). The random veto probability for the whole detector has to be of the order of 5% or less to have a negligible effect on the projected sensitivity.

The finalization of the design of the PADME charged-particle detector subsystem required the study of different scintillator surface treatments and light collection techniques, which will be discussed in Section III.

III. Prototype Construction

In order to study the properties of the components of the electron and positron veto subsystems, a special prototype was built. A picture of the prototype, mounted on the table for tests, is shown in Fig. 2, where the support frame, the scintillating bars, and the front-end electronics (FEE) cards are clearly visible.

In addition to the validation of the mechanical and electronic design, some variations in the light collection and scintillator treatment were also considered to find the optimal characteristics.

A. Scintillators

The prototype was constructed using extruded polystyrene-based scintillating plastic bars, with 1.5% *POPOP*, produced by *UNIPLAST*, Vladimir, Russia. The surface of the scintillators was covered with the chemical reflector. The scintillators were machined to have square transversal cross section with dimensions 10×10 mm^2. The nominal length of the scintillating bars for the construction of the charged-particle detectors is limited to 184 mm by the magnet aperture. Having in mind that the fine finishing on the optical contact needs to be guaranteed, scintillators with 200 mm length have been ordered. They will be shortened and polished together with the

glued fibers in their grooves. Longitudinally, the scintillators have a flat groove with cross section 1.3×1.3 mm^2. Since the extruded scintillators have shorter light attenuation length with respect to optical fibers, optionally a *BCF-92* wavelength shifting (WLS) fiber with $\varnothing$1.2 mm could be glued inside the groove. The maximal absorption of *BCF-92* is at about 400 nm, which matches up with the emission of POPOP scintillators. The emission of the fibers peaks at 492 nm and the absorption length for self-emitted light is $>$3.5 m.

B. Light Detection and Front-End Electronics

The strongest requirements for the photodetectors of the electron and positron veto subsystems are to be able to work inside vacuum and to sustain stationary magnetic field of 0.6 T. Silicon photomultipliers (SiPMs) were therefore chosen as photodetectors.

During the test beam, custom-designed FEE boards were used [9]. They were equipped with Hamamastsu 3×3 mm^2 silicon photomultipliers *S12572*. Although the photodetecting system had relatively long output signals $\mathcal{O}$(40 ns), its timing properties are determined by the pulse shape characteristics [10].

Each front-end channel includes a transimpedance amplifier with a factor of four gains and a buffer with differential output. It also includes a dedicated high-voltage regulation module, which is able to provide each SiPM with individually controlled supply voltage, as well as a circuit to monitor the applied voltage and the current flowing through the photodetector. The SiPMs are operated at the nominal voltage provided by the manufacturer for a gain of $\sim 5.5 \times 10^5$. Four FEE channels are grouped into one front-end card.

The signals from front-end cards are transferred to a dedicated controller which converts them into single ended signals drawn out to lemo.00 connectors on the front panel. This way, they are made suitable for the input stage of the chosen digitizing electronics. The controller handles up to four boards or 16 optical channels. It also manages the settings and controls the parameters of the individual FEE channels via I^2C communication, and is accessible from outside via Ethernet, using the embedded web-based interface.

During the PADME physics run, the FEE will be operated inside the vacuum chamber and in the magnetic field, while the controllers compliant with the NIM standard [11] will be located outside the vessel, close to the digital part of the data acquisition chain.

C. Prototype Construction

An aluminum support structure was built to hold a set of 16 scintillating bars together with the FEE boards. The frame also served as a mechanical prototype for the final detector construction. During the experiment the FEE boards will be located inside the vacuum chamber, which leads to heating complications. The proposed solution was to design the frame such that it transfers the heat to the surface of the vacuum chamber. This frame was used during the test beams in order to test for eventual influences of the behavior of the FEE boards.

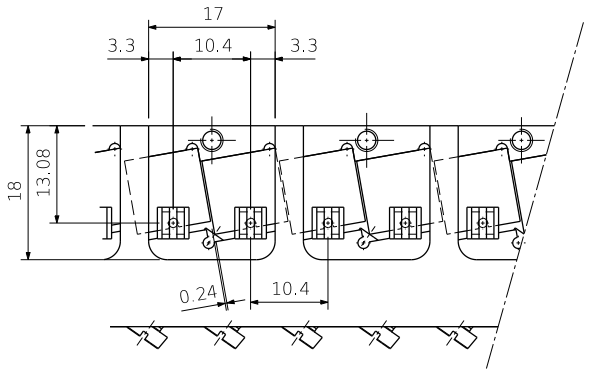

Fig. 3. Bottom view of the scintillator support structure. It is also visible how the SiPMs are centered over the WLS fibers and partially overlap the scintillators.

In order to reduce the geometrical inefficiency in the final design of the scintillating layer, a rotation of 0.1 rd around the long axis of the individual bars was considered (see Fig. 3). This concept was implemented in the studied prototype—milled aluminum rails of the support structure together with their screws—kept the scintillating bars secured in their positions while plastic endings on the edges prevented their finishing from being damaged.

The frame allowed the SiPM boards to be mounted in two different manners. The first one was to cover part of the scintillating bar surface only, while the second one was to cover the bar surface together with the groove or the WLS fiber, in case glued inside.

An additional cover, made of 8-mm-thick aluminum, emulated the electrical characteristics of the vacuum vessel, which might have some influence on the SiPM boards or communication lines.

WLS fibers of type *BCF-92* with diameter $\varnothing$1.2 mm were glued with *Eljen EJ500* optical epoxy cement in the grooves of some of the scintillating bars. The fibers featured short light decay time 2.7 ns, which is important for precise time measurements.

The scintillating bars were milled to the desired length. Then they were wet polished manually, one at a time, using the sequence of waterproof sandpapers of grits 80, 150, 300, and 800. It should be noted, however, that machine polishing or manual polishing in packets is preferable because single-bar manual polishing cannot guarantee flat surface of the scintillators.

The 16 counters have a parallelepiped shape, with dimension of $10 \times 10 \times 180$ mm^3. As shown in Fig. 4, they have been organized in groups of four counters for each FEE board, and are positioned one close to the others in a support structure, while keeping their long side perpendicular to the beam (z) direction. The first (channels 0–3) and the last (channels 12–15) groups were used to define an offline trigger based on their light output information to guarantee that at least a particle passed through the middle scintillators. The two middle groups (channels 4–8 and 11) were composed by scintillators with a different treatment and a different light collection, as shown in Table I.

All optical contacts were improved by using *Saint-Gobain BC-630* silicone optical grease.

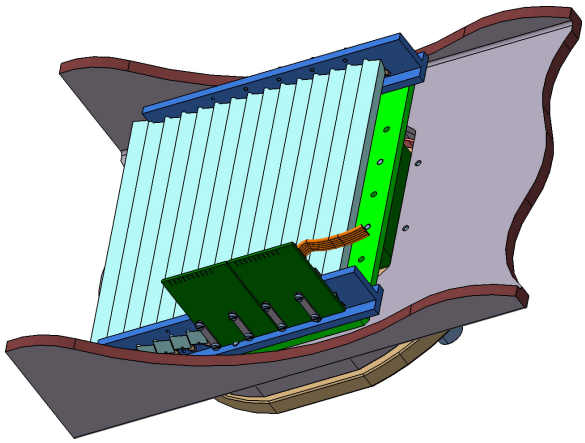

Fig. 4. Drawing of the studied prototype. The SiPMs, together with the PCBs (in green), are located over the WLS fibers. The head generated by the elements on the PCBs is transferred to the aluminum frame (light blue). The flange (in dark green) ensures a thermal coupling to the vacuum chamber (light gray).

TABLE I

CONFIGURATION OF THE SCINTILLATION BARS OF THE PROTOTYPE

RO Channel	Scintillator specs	Light collection
4 and 8	A fiber glued in the groove	Scintillator only
5 and 9	A fiber glued and aluminised	Fiber and scintillator
6 and 10	No fiber used	Scintillator only
7 and 11	A fiber glued in the groove	Fiber and scintillator

IV. TEST BEAM SETUP

The constructed prototype, together with its electronics, was tested at the beam-test facility (BTF), Frascati, Italy. The BTF is a dedicated transfer line of the DAΦNE Linac, which is able to deliver electrons and positrons in a dedicated experimental hall, used extensively for the detector testing purposes [7].

BTF has two main modes: "parasitic," when operated together with DAΦNE; and "dedicated," when the machine works only for providing beam to the BTF. The requirements of DAΦNE fix the pulse duration of the beam to 10 ns. The "parasitic" mode is also characterized with a reduced number of bunches delivered to BTF. When in "dedicated" mode, the restrictions set by DAΦNE are no longer applicable which results in ability to use all the 49 bunches/s and to vary the beam duration from 1.5to 150 ns. In this mode, it is also possible to accelerate the beam to higher energies.

The beam transport line is designed such a way that it can deliver primary beam with higher intensities and energy of 510 Mev to the BTF, or deliver secondary beam with variable energies and intensities.

During the test beam, the machine was configured to provide the same beams for both "parasitic" and "dedicated" modes with the following properties: $\mathcal{O}(1)$ particle per pulse, beam energy of 500 MeV, and pulse duration of 10 ns. Modifications to the BTF are foreseen to make it suitable for PADME [6].

The test beam setup is shown in Fig. 5 and more details are given as follows.

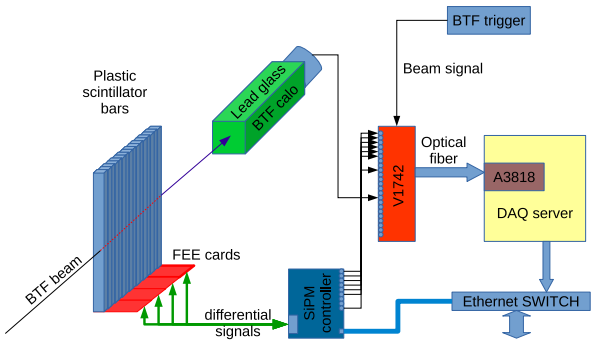

Fig. 5. Schematics of the test beam setup.

A. Installation

The prototype was placed on a remotely controlled table inside BTF hall and the bars were impinged transversally with the electron beams.

A lead-glass calorimeter (BTFCalo), placed downstream, was used to reconstruct the total beam energy in a single pulse, providing information about the number of the particles per bunch. In addition to the requirement for single particle in the beam, guaranteed by BTFCalo, the offline trigger also demanded at least four scintillators to have signal (two upstream and two downstream with respect to the studied scintillators) but none of the scintillators had the signal corresponding to more than one particle.

Data for nine equidistant positions of the beam along scintillating bars were taken. The longitudinal scan started at 10 mm and ended at 170 mm of the bar, measuring from the SiPM side. This allowed a detailed study of the performance of the charged-particle detector prototype.

B. Data Acquisition System

The data acquisition was realized using a 32-channel switched capacitor sampling digitizer (*CAEN V1742*) operated at 5 GS/s.

All waveforms from the SiPM were digitized together with the lead-glass calorimeter signal. A trigger signal according to the NIM standard[1] was provided by the BTF, upon the beam arrival, thus introducing no bias to the data collection. The data from the digitizer were transferred through *CONET2* optical connection, based on *CAEN A3818*, providing galvanic decoupling, high bandwidth, and the possibility to connect several digitizers in a daisy chain. Development versions of the general PADME software for process control and data collection were run on a blade server. The data were stored in binary-format files, containing the sequence of the recorded events. Each event contained sequences of the values of the digitized amplitudes of the signals for all the enabled channels. The data acquisition window was 1024 samples (200 ns in 5-GS/s mode). These nonzero-suppressed data also allow precise pedestal and timing calibration.

V. EVENT RECONSTRUCTION

A. Charge Reconstruction

A typical set of waveforms for one of the recorded channels is shown in Fig. 6.

[1]The logical "1" is defined as -16 mA or -0.8 V over 50-Ω input impedance, DOE/ER-0457T.

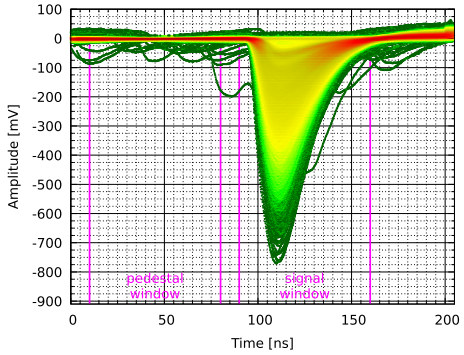

Fig. 6. Cumulative plot of typical signals from one of the channels. The multiparticle events are not filtered out this plot. Pedestal range: 10–80 ns. Signal range: 90–160 ns.

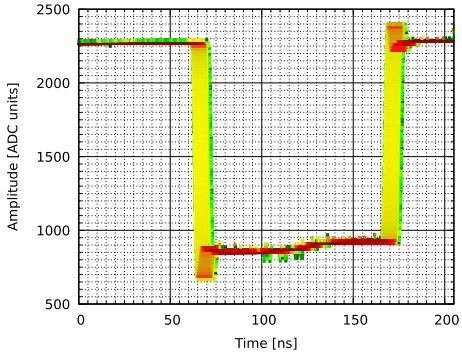

Fig. 7. Cumulative plot of the triggers.

Two equal-width windows were defined along the recorded waveforms. One covering the region where the beam-related signals are expected to arrive and another one covering a pedestal-only region. The former is used to study the light properties of the studied prototype, while the latter is used to calculate the pedestal for each event but also for noise studies. Equal-width time windows were preferred as this leads to a simplification in noise/efficiency analysis. The median of the samples is used as a pedestal estimate since accidental SiPM activity in the pedestal window may induce a shift in the mean value and bias the result. The pedestal jitter follows a Gaussian distribution with $\sigma = 5 \div 8$ ADU (ADC units). An offset of 1 ADU integrated over the peak window results in about 1 Phe$^-$. This defines the need to compute the pedestals for each event individually but not once per run.

All values of the pedestal-corrected waveforms, falling in the later time window—assuming 50 Ω input impedance of the digitizer and known SiPM and FEE gains—were used to calculate the number of SiPM pixels having signal, later denoted as Phe$^-$.

B. Time Reconstruction

Different methods for estimating the signal timing were studied. They were based on using either only the information of the rise time of the signal, or employing the full signal shape. The considered timing algorithms are briefly listed as follows.

- *Constant Fraction:* The time of reaching a constant fraction of the signal maximum amplitude was estimated with

$$t_{\mathrm{Max}_F} : A_{t_{\mathrm{Max}_F}-1} \leq F \times \max_{i \in \mathrm{Peak}} A_i < A_{t_{\mathrm{Max}_F}} \qquad (3)$$

  where F is a constant which takes values 0%, 10%, 20%, 50%, and 100%.
- *Weighted Mean Time:* The weighted mean time was calculated using the full information for the signal profile, according to

$$t_{\mathrm{Mean}} = \frac{\sum_{i \in \mathrm{Peak}} B_i \times i}{\sum_{i \in \mathrm{Peak}} B_i} \qquad (4)$$

  where the used amplitude B_i may be the amplitude samples themselves ($B_i = A_i$), the amplitude squared ($B_i = A_i^2$), or the absolute value of the amplitude ($B_i = |A_i|$).
- *Integral Ratio:* The time in this method was defined as the moment when the collected charge in the pulse reaches a fraction M of the total charge in the pulse. This moment can be calculated as

$$t_{\mathrm{Int}} : \sum_{i \in \mathrm{Peak}}^{t_{\mathrm{Int}}-1} A_i \leq M \times \sum_{i \in \mathrm{Peak}} A_i < \sum_{i \in \mathrm{Peak}}^{t_{\mathrm{Int}}} A_i \qquad (5)$$

  where M is the constant. Again, as in the case of the weighted mean method, the calculation of t_{Int} uses information for the whole signal pulse. Best results were obtained for $M = 0.115$.
- *Line Approximation:* For signals with fast rise time, a line approximation can be used to determine the start of the signal. Three different time definitions using the leading and trailing edges of the signals approximated with straight lines passing through 20% and 80% of the maximum value were used. They were the leading edge extrapolated to "zero" amplitude; the interpolation to 50% of the maximum amplitude; and the point where the approximations for the leading and the trailing edge cross, which should correspond to the time of the peak of the signal.

Due to architecture specifics in the digitizer module *V1742*, the time in separate events jitter. However, *V1742* module allows the input trigger signal to be digitized together with the rest of the channels. A cumulative plot of the digitized triggers is shown in Fig. 7. The jitter follows an uniform distribution of about ±20 samples (±4 ns) wide. An offline time correction was applied using a fixed threshold algorithm, with discrimination level set at 1500 ADU. The time offsets calculated with this method were applied to all digitized channels to account for the time jitter.

C. Particle Counting

The signals from the lead-glass calorimeter were used to determine the number of particles in every beam pulse. A spectrum of the reconstructed charge in the BTFCalo is shown in Fig. 8. The peaks for events with single, double, multiple, or without any particle in the event are clearly separated.

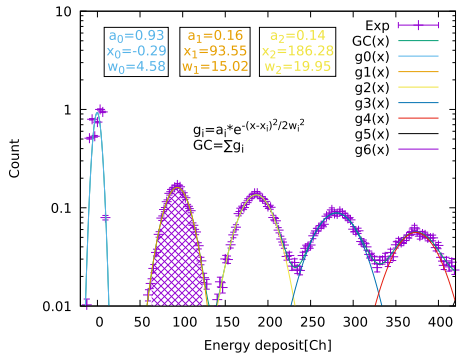

Fig. 8. Total energy deposit in BTFCalo. Peaks are fit with the sum of Gaussian functions. The filled area under the second peak (single electron bunches) shows the boundaries used in the offline trigger.

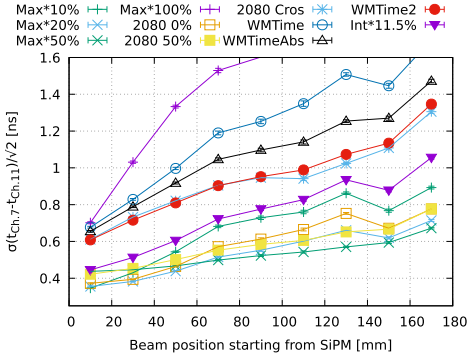

Fig. 9. Time resolution comparison. The same data for channels 7 and 11 are analyzed using various definitions for "event time". Timings for Max*10%, Max*20%, Max*50%, and Max*100% are calculated with the constant fraction method; 2080 0%, 2080 50%, and 2080 Cros: line approximation; WMTime, WMTimeAbs, and WMTime2: weighted mean time, calculated for the signal itself, the signal by absolute value, and the signal squared, respectively; Int*11.5%: integral ratio at $M = 0.115$.

A sum of Gaussian functions $\mathrm{GC} = \sum g_i$, was fit to the energy spectrum, where g_i corresponds to the Gaussian charge distribution in the case of i electrons deposit their energy in the BTFCalo. The first peak in Fig. 8 corresponds to empty bunches, the second to single electron bunches, and so on.

Defining a range for single electron selection centered around the single particle peak (93.55±30 channels), results in an acceptance for single particle beams of 95.47%, and probability to have the contamination of 0 or 2 or more electron beams as low as 0.096%.

VI. Results and Discussion

Both the time resolution and the efficiency were studied as a function of the impact point of the beam along the bar axis. The analyzed events were required to have exactly one particle in the beam and to have hits in two out of four scintillators both upstream and downstream.

A. Time Characteristics

Since multiple definitions of the "event time" were considered, the optimal one is that providing the best time resolution between the two plastic scintillator channels under examination. The time resolution obtained for a given light collection scenario using the different time reconstruction techniques, is shown in Fig. 9, as the function of the distance of the beam

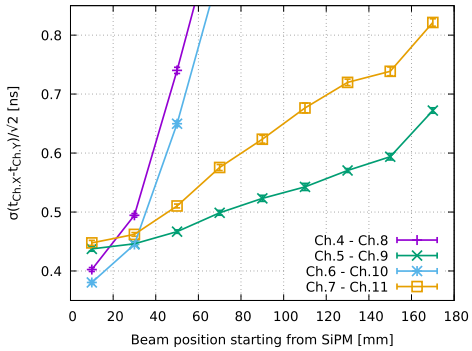

Fig. 10. Time resolution comparison for different scintillator light collection types. Max*50% is used as the time reconstruction method.

impact point on the scintillator from the SiPM. Using the fact that the two scintillators (channels 7 and 11) have the same treatment and the same properties are expected, the resolution was normalized for a single channel by dividing by $\sqrt{2}$.

The dependence of the time resolution from the longitudinal position is explained by the increased light, and correspondingly photoelectric yield, reaching the SiPM, when the beam impinges on the bar at short distance from the SiPM. The methods which rely predominantly on the rising edge information provide the best timing resolutions reaching values down to 600 ps and better. The most stable technique appears to be the "event time" defined as the half of the maximum of leading edge. This was used to obtain the results shown as follows.

Fig. 10 shows the longitudinal dependence of the time resolutions for scintillating bars having different scintillator treatments and light collections. The analysis is based on all possible time differences between the events in two identical bars. Since there is no obvious reason leading to a nonsymmetric time distribution, this was fit with a Gaussian curve. The value corresponding to the standard deviation is reported as the time resolution for a single channel.

The solution without WLS fibers (Fig. 10) is above the threshold of 1-ns time resolution for particle impact point further than 7 cm from the photodetector. Since most of the charged particles in PADME cross the scintillator bars in the middle (located at ∼9 cm from the photodetector) this design was ruled out. The decrease in the time resolution was due to the decreased amount of collected light since it is a result of multiple reflections on the scintillator edges, which were treated to provide diffuse reflection. This resulted in shorter effective light attenuation length. The assembly with WLS fibers provides time resolution better than 1 ns for the whole scintillator length and this matches the PADME charged-particle veto design requirements. That is why it was decided to adopt this solution in the final detector construction.

B. Noise and Efficiency

Other important parameters related to the veto system are the efficiency and the probability to veto on random signals. Threshold scans of noise and inefficiency helped to select a threshold of 10 Phe^-, which was used to consider a hit was presented in the given channel.

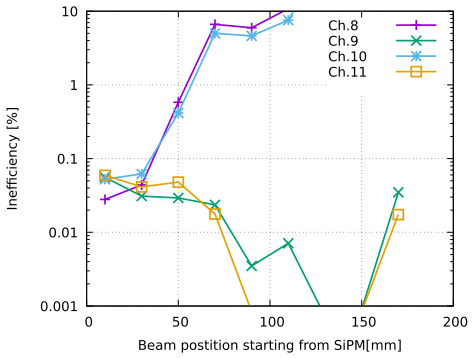

Fig. 11. Inefficiency as a function of the particle impact point along the scintillator for a fixed threshold of 10 Phe$^-$.

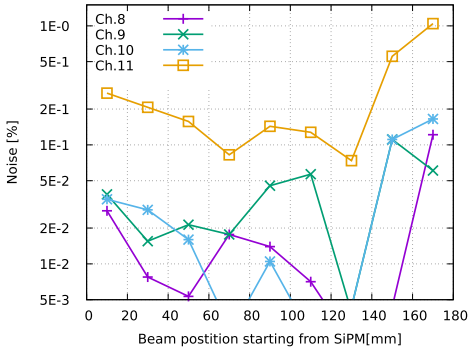

Fig. 12. Noise at fixed threshold of 10 Phe$^-$.

The efficiency, in this paper, is defined as the ratio between the number of events in which the detector had signal bigger than 10 Phe$^-$ with respect to the number of events, satisfying the trigger requirements.

As shown in Fig. 11, the inefficiency depends dramatically on the WLS fibers. For the scintillating bars with scintillator only light collection an efficiency >99.95% is obtained only in the first 30 mm from the SiPM. In all other positions these scintillators are incompatible with PADME requirements.

On the other hand, the scintillators with fiber light collection show an efficiency higher than 99% and uniform along the bar results. Efficiencies in the practical region around 100 mm are higher than 99.98%.

Noise corresponds to the events which show signals with no particle passing through the scintillators. Fig. 12 shows the probability for false positive events within a time window of 70 ns. This probability is not expected to depend on the scintillator treatment or the presence of WLS fiber. It was observed, however, that one of the channels was noisier than the others. The reason for that is not fully understood, but problems with the electronics are suspected. The rest of the channels show noise probability of 5×10^{-4}, for a 70-ns time interval. Using a conservative estimate $\sigma_{\text{veto}} = 1$ ns and taking $\pm 2\sigma$ time window around the event time as defined by the time of the detected photon in the calorimeter and a system of 200 detecting elements, the total probability to have a random event in the charged-particle veto amounts to $\sim 5 \times 10^{-3}$. Being one order of magnitude lower, this value is consistent with the PADME requirements.

VII. Conclusion

The presented measurements were performed with a prototype of PADME veto detector during April 2017 at the BTF at Laboratori Nazionali di Frascati of INFN.

Results for particle detection efficiency and time resolution obtained with plastic scintillators with different treatments and different light collection schemes were compared.

The plastic scintillating bars with glued WLS fiber show efficiency and random noise acceptable for the experiment. The silicon photomultipliers and the prototype read-out electronics used during the tests prove to be able to provide the needed time resolution for the experiment. The detector is currently under construction with the chosen technology based on the outcome of presented results and is expected to be finalized by the end of March. This is in line with the foreseen PADME operation starting by the end of April, 2018.

Acknowledgment

The veto team acknowledges the BTF team for the provided beam time and the support during the tests, the support of C. Capoccia for the design of the frame, and G. Corradi for the design of the SiPM boards and the module for SiPM control.

References

[1] M. Raggi and V. Kozhuharov, "Results and perspectives in dark photon physics," *Rivista Nuovo Cimento*, vol. 38, no. 10, pp. 449–505, 2015.

[2] M. Raggi and V. Kozhuharov, "Proposal to search for a dark photon in positron on target collisions at DAΦNE linac," *Adv. High Energy Phys.*, vol. 2014, Jul. 2014, Art. no. 959802. [Online]. Available: http://dx.doi.org/10.1155/2014/959802

[3] M. Raggi, V. Kozhuharov, and P. Valente, "The PADME experiment at LNF," in *Proc. EPJ Web Conf.*, vol. 96. Jul. 2015, p. 01025.

[4] G. Chiodini, "A diamond active target for the PADME experiment," *J. Instrum.*, vol. 12, no. 2, p. C02036, 2017.

[5] M. Raggi *et al.*, "Performance of the PADME calorimeter prototype at the DAΦNE BTF," *Nucl. Instrum. Methods Phys. Res. A, Accel. Spectrom. Detect. Assoc. Equip.*, vol. 862, pp. 31–35, Aug. 2017.

[6] P. Valente *et al.* (Mar. 2016). "Linear accelerator test facility at LNF conceptual design report." [Online]. Available: https://arxiv.org/abs/1603.05651

[7] G. Mazzitelli, A. Ghigo, F. Sannibale, P. Valente, and G. Vignola, "Commissioning of the DAΦNE beam test facility," *Nucl. Instrum. Methods Phys. Res. A, Accel. Spectrom. Detect. Assoc. Equip.*, vol. 515, no. 3, pp. 524–542, 2003.

[8] V. Kozhuharov, "Background in the search for dark photon in e^+e^- annihilation," in *Proc. EPJ Web Conf.*, vol. 142, p. 01018, Apr. 2017.

[9] G. Corradi *et al.*, "Charged veto electronics," in *Proc. PADME General Meeting*, Jan. 2017.

[10] I. Antonova *et al.*, "A test system for the front-end electronics of the PADME charged particle detector system," in *Proc. 26th Conf. Electron.—ET*, 2017, p. 277, doi: 10.1109/ET.2017.8124360.

[11] *Standard NIM Instrumentation System*, document DOE/ER-0457T. [Online]. Available: http://www.osti.gov/energycitations/servlets/purl/7120327-MV8wop/7120327.PDF